

# New Bone Formation and Microstructure Assessed by Combination of Confocal Laser Scanning Microscopy and Differential Interference Contrast Microscopy

Xiaohong Yang · Ling Qin · Weiguo Liang ·  
Wen Wang · Jianrong Tan · Peihong Liang ·  
Jiake Xu · Siming Li · Shuliang Cui

Received: 23 July 2013 / Accepted: 24 October 2013 / Published online: 20 November 2013  
© Springer Science+Business Media New York 2013

**Abstract** Bone is a mineralized connective tissue that is continuously and microstructurally remodeled. Altered bone formation and microstructure arise in pathological bone conditions such as osteoporosis, osteonecrosis, fracture repair, and Paget disease of bone. A proper and objective assessment of bone formation and microstructure will provide insight into the understanding of bone pathogenesis and remodeling. Here, new bone formation *ex vitro* and its microstructure were evaluated in *in vivo* multiple sequential polychrome-labeled samples using confocal laser scanning microscopy (CLSM), which generated clearer and more reliable images of thick bone sections than conventional fluorescence microscopy (CFM). Intriguingly, fine details of the bone microstructural features, including the mineralization fronts, quiescent versus active osteons, and Volkmann's channel, were elucidated using CLSM, which defines the relationship between

morphological changes and function, when combined with differential interference contrast microscopy. Furthermore, CLSM provided objective evaluations of bone formation, such as the ratio of labeled areas of new bone formation in a rabbit model when compared with CFM. Altogether, new bone formation and its microstructure can be evaluated more adequately using a combination of CLSM and DIC microscopies.

**Keywords** Confocal laser scanning microscopy · Fluorescence labeling · Differential interference contrast microscope · New bone formation · Microstructure

## Introduction

Bone is a mineralized connective tissue that contains cortical and trabecular components and is continuously and

---

The authors have stated that they have no conflict of interest.

---

X. Yang (✉) · W. Liang · W. Wang · J. Tan ·  
P. Liang · S. Li · S. Cui  
Guangzhou Institute of Traumatic Surgery, The Fourth Affiliated  
Hospital, Jinan University School of Medicine, 396 Tong Fu  
Zhonglu Road, Hai Zhu District, Guangzhou 510220,  
Guangdong, People's Republic of China  
e-mail: dryang1192@tom.com

X. Yang · L. Qin  
Musculoskeletal Research Laboratory, Department of  
Orthopaedics and Traumatology, Chinese University of Hong  
Kong, Shatin, NT, Hong Kong SAR, People's Republic of China

L. Qin  
Translational Medicine Research & Development Center,  
Institute of Biomedical and Health Engineering, Shenzhen  
Institutes of Advanced Technology, Chinese Academy of  
Sciences, Shenzhen 518055, People's Republic of China

J. Xu (✉)  
School of Pathology and Laboratory Medicine, University  
of Western Australia, Crawley, WA 6009, Australia  
e-mail: jiake.xu@uwa.edu.au

S. Cui (✉)  
Department of Zoology, University of Melbourne, Parkville,  
VIC 3010, Australia  
e-mail: s.cui2008@gmail.com

microstructurally remodeled under physiological conditions. Abnormal bone formation and microstructure arise in pathological bone diseases. A more precise progressive evaluation of bone formation and microstructure will facilitate the diagnosis and treatment of bone diseases.

The mineralization front of bony ossification surfaces in new bone formation is commonly labeled using tetracycline and other fluorescent agents. The bone apposition rate in new bone formation can be calculated when polychrome sequential labeling is employed by *in vivo* administration of fluorescent agents, either orally or intravenously [1–4]. Relatively large histological thick sections of 100–300  $\mu\text{m}$  are prepared from nondecalcified bone embedded in methylmethacrylate and/or a series of thin sections (8–20  $\mu\text{m}$ ), which requires a special heavy-duty microtome for preparation in conjunction with the process of evaluation of the specimens, is time-consuming [5–7], and is technically inevitably needed for achieving quality images to visualize the fluorescent labeling under the conventional fluorescent microscope (CFM) for analysis without partial volume effect (PVE); i.e., images are hampered by the loss or underestimation of apparent activity in small objects/regions from the finite spatial resolution of imaging systems where detected photons originating at locations within the tissue are blurred into surrounding locations in close proximity during data acquisition [8, 9].

Confocal laser scanning microscopy (CLSM) is a technique for obtaining high-resolution optical images through a process of controlled optical sectioning with highly limited depth of focus by selection, only one depth level at a time and, assisted with a computer, point by point to reconstruct 3D images of topologically complex objects with nonsuperimposed interior images at multiple depths over conventional microscopy, which visualizes as the light penetrates [10]. CLSM enables the 3D assessment of the cell–matrix information layer by layer in a noninvasive manner for thick tissue samples without mechanical sectioning [11, 12]. Sequential images were obtained from rat samples of transforming growth factor- $\beta$  implant for promoting new bone formation in the cranium and iliac bone and used to calculate the rate of bone formation [12]. Comparisons of sections of unstained fresh samples and hematoxylin and eosin–stained sections were made between CFM and CLSM [13].

A study using CLSM on the mineralization of articular cartilage in racehorses simultaneously detected two important parameters with high repetitiveness: the linear growth rate and fluorescence density [14]. Bisphosphonates and related drugs, such as risedronate and its lower-affinity analogues deoxyrisedronate and 3-(3-pyridyl)-2-hydroxy-2-phosphonopropanoic acid, bind to calcium with different affinities for bone mineral at resorbing surfaces and

forming surfaces, which differs from that observed at quiescent surfaces. The distribution of fluorescently labeled calcium binders of various affinities were detected, revealing the effects of their bone mineral affinity within the skeleton [15]. Moreover, pulsed with calcein, alizarin complexone, and tetracycline, bone formation around hydroxyapatite implants in normal and diabetes mellitus (DM) animals at various times after implantation was scanned with CLSM and showed different patterns in the normal group versus the DM group [16]. Using dual staining of fluorescent calcein and alizarin red at different times, temporal patterns of bone formation were accurately assessed by CLSM in undecalcified thick sections with titanium implants left *in situ* and profiled the bone first formed as thin processes toward and across the implant surface, followed by further development with a space in the bone–implant interface [17]. Overlapped with high-resolution imaging of surfaces with compositional information acquired by back-scattered electron detector (BSE) combined with scanning electron microscopy, CLSM scanning filled the gap of cells and osteoid left by BSE to rebuild the cellular localization in bone samples embedded in polymethylmethacrylate [18].

CLSM was used quantitatively in single-molecule imaging based on fluorescence intensity distribution for statistical analysis of molecular occurrence in different forms, including DNA and proteins in solution [19]. CLSM was also used for subcellular analysis in fungi [20], for host–fungus interactions and spatial patterns of colonization, and for obtaining sharp images of fungi within a host or colonizing highly contoured or rugged surfaces [21]. Fluorescence of a visible-wavelength  $\text{Ca}^{2+}$ -sensitive fluorophore in isolated cardiac myocytes was visualized using CLSM as a measurement of intracellular calcium changes occurring in spontaneously active cardiac cells [22].

We used 3D structural imaging and quantitative characterization in thick tissue based on CSLM and derivative techniques in quantitative imaging of biomolecular localization and trafficking in live cells [23]. Fluorescent signals in cartilage of cryostat sections of mouse articular cartilage were quantified by localizing and quantifying insulin-like growth factor-1 (IGF-I) receptor expression *in situ* using CLSM to analyze its distribution patterns in chondrocytes [24], which was further applied in quantitative analysis of *in situ* localization patterns of the IGF-I receptor in a normal or arthritic intact patellae murine model [25]. These results showed the powerful capability of CLSM in elucidating the cellular structure and function of bone tissues. When CLSM is linked to differential interference contrast (DIC), it is technically possible to obtain clear fluorescently labeled images with the assistance of transmitted light for an accurate localization of the fluorescent dye on the bone surface.

In this study, new bone formation and bone microstructure, including mineralization fronts, quiescent vs. active osteons, and Volkmann's channel, in thick bone samples were assayed using DIC combined with CLSM to generate fluorescent images of high resolution that could be used to quantitatively assess the progressive mineral deposition of bone growth.

## Materials and Methods

### Polychrome Sequential Labeling of Bone In Vivo

The fluorescent agents calcein green (excitation 488 nm) and xylenol orange (excitation 453 nm) (Sigma, St. Louis, MO) were prepared in phosphate buffer (pH 7.2), sterilized, and filtered for in vivo injection at a dose of 10 mg/kg and 90 mg/kg, respectively.

Four adult female Chinese goats,  $26 \pm 3.2$  kg, were injected with fluorescent dyes intravenously once every 2 weeks four times prior to sample collection, with an injection sequence of calcein green  $\rightarrow$  xylenol orange  $\rightarrow$  calcein green  $\rightarrow$  xylenol orange [26]. Longitudinal sections of tibia were prepared to observe the effects of multiple fluorescent labeling in images acquired by CLSM. Transected samples were also prepared to investigate the relation between bone surface structure and bone mineral deposition labeled with fluorescence using DIC.

A partial patellectomy model in rabbits was employed as previously described [27] to assess bone formation using CFM and CLSM. Four 18-week-old adult female New Zealand rabbits,  $3.5 \pm 0.5$  kg body weight, were anesthetized using 10 % ketamine (0.5 mL/kg) i.m. and 2.5 mL 2.5 % phenobarbitone sodium i.v.; then, the distal one-third of woven bone was transversely sectioned and removed, and two 0.8-mm pores were perforated vertically to the proximal end of residual woven bone. The patellar ligament was directly stitched onto the proximal woven bone with a nonabsorbable suture, which was protected with no. 8 steel thread, and fixed in position using gypsum for 6 weeks with the position of the knee joint at 90° flexion. The operation sites were given low-intensity pulsed ultrasound (LIPUS) treatment at day 3 after the operation using the physical parameters as detailed previously [27–29], to enhance bone healing up to the twelfth week after operation. Following the surgery, the animals received calcein green and xylenol orange s.c. once every 2 weeks and were killed 3 days after the last injection; woven bones were longitudinally sectioned for evaluation of the optical density of mineralized areas and quantitation of new bone formation rate. For animal ethics, approval was obtained from The Fourth Affiliated Hospital, Jinan University School of Medicine, prior to the experiments.

### Sample Preparations

All samples were fixed in 10 % neutral formalin solution, dehydrated in a graded series of ethanol, and embedded in methylmethacrylate. Bone specimens were sectioned using a saw microtome (SP1600; Leica, Solms, Germany) at a thickness of 400  $\mu$ m for goat samples and 300  $\mu$ m for rabbit samples according to our established protocol [30].

### CFM

Fluorescent images were obtained using a fluorescent microscope (Axiovert 200 M; Zeiss, Göttingen, Germany) equipped with a high-voltage mercury lamp, a green broadband filter disk (#9, Zeiss), and a red broadband filter disk (#15, Zeiss). The overall histological structure of bone tissues was viewed under low magnification (1.25 $\times$ ), and the fluorescence-labeled line of calcification fronts was observed under high magnification (40 $\times$ ) using the Digital Color charge coupled device and Digital Video (Camera AxioCam MRc Rev. 2, 1,388  $\times$  1,040; Zeiss). The tissue structure was displayed and evaluated using the Microscopic Image Analysis System (AxioVision Rel. 4.5 Software, Zeiss).

### CLSM

Images were acquired using the multi-tracking scan (MTS) mode and MTS with transmitted light mode (Zeiss LSM 510 META system) with excitation wavelengths of 488 and 453 nm for calcein green and xylenol orange, respectively, and emission wavelengths of 520 and 615 nm for calcein green and xylenol orange, respectively, as previously described [5].

In MTS mode, single-layer images were acquired using dual fluorescent tracks of green for calcein green and red for xylenol orange and analyzed using the conventional histomorphometric method of bone remodeling or apposition rate, which measures the distance between two fluorescent labels generated by timed injection and divided by the number of days between injections to give the rise of an average growth rate, i.e., distance (micrometers)/days [1, 2, 31], and the estimation of new bone formation, in which region of interest (ROI) was selected using the image analysis software for quantifying two different fluorescent dyes by calculating mean fluorescence-labeled areas for calcein green and xylenol orange as the reported index of new bone formation rate [27]. New bone formation in repairs was estimated by comparisons of the areas (micrometers  $\times$  micrometers) of red and green fluorescence labels in the ROI obtained using the image analysis software (LSM 510 Release Version 4.0 SP2; Zeiss), in which the fluorescent dyes were quantified in pixels as

mean intensity with a standard derivation and converted into areas, to those in the control group so that the background noises were eliminated. The ratio of the mean fluorescence labeled area by calcein green over the mean area labeled by xylenol orange was used as the bone formation rate in the new bone region of patellectomy repair in this study.

Thick samples were optically sectioned in the ROI to obtain 131 continuous images of  $225\ \mu\text{m}$  ( $x$ )  $\times$   $225\ \mu\text{m}$  ( $y$ )  $\times$   $0.51\ \mu\text{m}$  ( $z$ ), and those images were sequentially overlapped along the  $z$ -axis with a suggested optimal interval of 0.5 to form a stack of  $225\ \mu\text{m}$  ( $x$ )  $\times$   $225\ \mu\text{m}$  ( $y$ )  $\times$   $65.99\ \mu\text{m}$  ( $z$ ) in CLSM using a laser pointing beam with no damages to the block, which allowed real 3D reconstruction (as detailed in the *Zeiss Operating Manual*, Zeiss). Images were manipulated and viewed using the CLSM image analysis software Physiology/Timeseries for Release 4.0.

### Statistical Analysis

One-way ANOVA in the SPSS13.0 software package was adopted to perform the statistical analyses of digitized quantitative data.

## Results

### Comparative Imaging Analysis of Bone Formation by CFM and CLSM

Comparison of fluorescent dye signals in images of thick sections of goat tibial bone that received four sequential injections of calcein green  $\rightarrow$  xylenol orange  $\rightarrow$  calcein green  $\rightarrow$  xylenol orange showed clear differences between CFM and CLSM. In the image acquired by CFM with  $>100\times$  magnification, an indistinct connection of fluorescent labels accompanied by intercrossing and interfering signals was observed above and below the focal plane of the labeled bands in a typical section (Fig. 1a), which gave blurry labeling lines of the calcification front. In the same ROI, sharp labeling lines from the four distinct dye bands showed no interference in the image acquired by CLSM (Fig. 1b), indicating that the imaging quality of fluorescently labeled thick bone sections generated by CLSM was much higher than that by CFM.

The CLSM optical scanning with a thickness of  $0.51\ \mu\text{m}$  was adjusted along the longitudinal section of goat tibial bone at a depth of  $65.99\ \mu\text{m}$  to obtain images with the required signal brightness of fluorescent labels [32]. The bone tissue block was scanned by CLSM in an ROI of  $225\ \mu\text{m}$  ( $x$ )  $\times$   $225\ \mu\text{m}$  ( $y$ ) from the surface layer to the deep layer to generate sequential single optical microscopic

sections (Fig. 1b). The sectioning was moved longitudinally ( $z$  axis) across a whole osteon with an optimal interval of 0.5 to obtain optical section images for 3D reconstruction showing the spatial structure of the bone formed (Fig. 1c). The measurement of thick bone sections represented new bone formed within the ROI of whole samples with no limitation just to the surface layer. By dragging a cross mark at the center of the figure to any position on the image, the depth of calcification labels in the sample block was shown by inserted thumbnails on the top and side figures (Fig. 1d), which illustrated the distribution of deposited calcium in the process of bone formation in 3D that cannot be done by CFM.

### Improved Assessment of Bone Formation by CFM and CLSM Using a Partial Patellectomy Model in Rabbits

The patella is a sesamoid bone embedded within a ligament in the knee joint and maintains a quiescent state for bone mineral apposition in adult rabbits normally, with both ends attached to the tendon displaying fluorescent labels of the mineral deposition as observed by CFM under low magnification (Fig. 2a). Twelve weeks after the partial patellectomy in the LIPUS treatment, the patella was in an exuberant bone metabolic process, especially in new bone forming areas where the fluorescently labeled mineral became more obvious, indicative of increased bone remodeling activity as visualized by CFM (Fig. 2b). Moreover, the newly formed bone was labeled in stronger green than the overlapped red labels (Fig. 2f–h), while the fluorescent labeling in the old bone area displayed a regular pattern of fewer overlapped green and red labels (Fig. 2i–k). Substantially overlapped dual-colored labeling bands were seen by CLSM scanning in the new bone formation (Fig. 2h), but few locations were visible across the region with the widest point of  $20.85\ \mu\text{m}$  (Fig. 2c, e). The new bone growth rate according to the traditional measurement of distance was calculated as  $20.85\ \mu\text{m} \div 14\ \text{days} = 1.49\ \mu\text{m}/\text{days}$ . Multiple locations of dual-colored mineral labels with the widest point of  $34.31\ \mu\text{m}$  (Fig. 2d, e) were recorded in the old bone region, and its growth rate was calculated as  $34.31\ \mu\text{m} \div 14\ \text{days} = 2.45\ \mu\text{m}/\text{days}$ , which is higher than that of the new bone formation. There seemed to be irregular patterns of fluorescent labeling in new bone tissues. The new bone growth rate was obtained by comparison of the calcein green- and xylenol orange-labeled areas in images acquired by CLSM with coordinate adjustment of operating parameters, such as the laser power of transmission, pinhole diameter, thickness of optical sectioning, and detector gain, for conformational evaluation of the new bone growth rate (Fig. 2l). The new bone growth

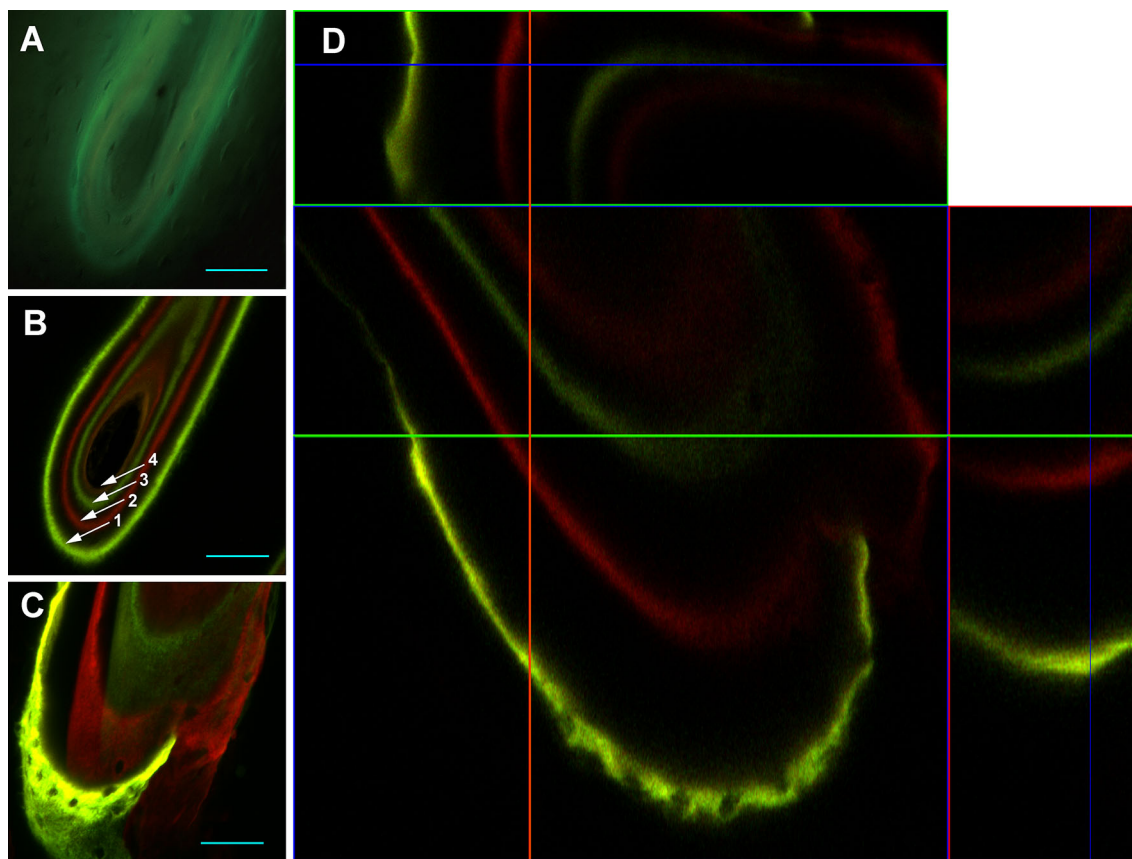


**Fig. 1** Comparative analysis of polychrome sequentially labeled images by two different microscope systems. Longitudinal section of goat tibia with a thickness of 400  $\mu\text{m}$ , scale bars 50  $\mu\text{m}$ . **a** Conventional fluorescence microscope (CFM) image, with four broad and partially overlapping labeled lines that cannot be used for a precise quantification of bone apposition rate (measurement of the distance between lines). **b** Confocal laser scanning microscope (CLSM) image. Arrows 1–4 indicate labeled lines generated by four sequential

intravenous fluorescent dye injections of calcein green  $\rightarrow$  xylenol orange  $\rightarrow$  calcein green  $\rightarrow$  xylenol orange. **c** A 3D image constructed by superimposing single-layer optical sections acquired in **b**. **d** Orthogonal sectioning of **b**, stacks in three cut views of  $xy$ ,  $xz$ , and  $yz$ . The  $xz$  image was flipped up and the  $yz$  image was laterally flipped on the right of the  $xy$  image, showing the mineralization detected in three dimensions

rate agreed with the intensity of fluorescent labels observed by microscopy.

#### Improved Visualization of Bone Microstructure by CLSM in Combination with DIC Microscopy

The MTS images of fluorescence labeling signals were obtained by CLSM (Fig. 3a, b) and coalesced by DIC transmitted light images to accurately localize the microstructure of the labeled bone matrix for fluorescence measurement. The mineralization fronts of osteons were localized in bone samples, and their relationships with bony structures around the fluorescent labels were clearly shown with static and active osteons visible simultaneously within ROI (Fig. 3c). Quiescent osteons were observed with no fluorescent signals, while active osteons were labeled with dual fluorescence. The images were merged to show their mineral calcification activity, notably, Volkmann's channels

were also visualized in compact bone and run perpendicularly to the haversian canals (Fig. 3d).

#### Discussion

CLSM is an advanced imaging technology developed in the 1980s and has gradually become popular in all biological and medical research fields. CLSM uses a laser as a light source with penetration ability based on optical confocal technology combined with a laser scanning device attached to the fluorescence microscope to obtain images that are manipulated by a computer to produce higher-quality images than CFM. The application of laser, confocal imaging, and pinhole prevented interference from diffracted light and scattered light; the MTS function ensures enough fluorescent signals, especially weak fluorescent light signals, and eliminates crosstalk between samples so that MTS scan samples with multiple labels at

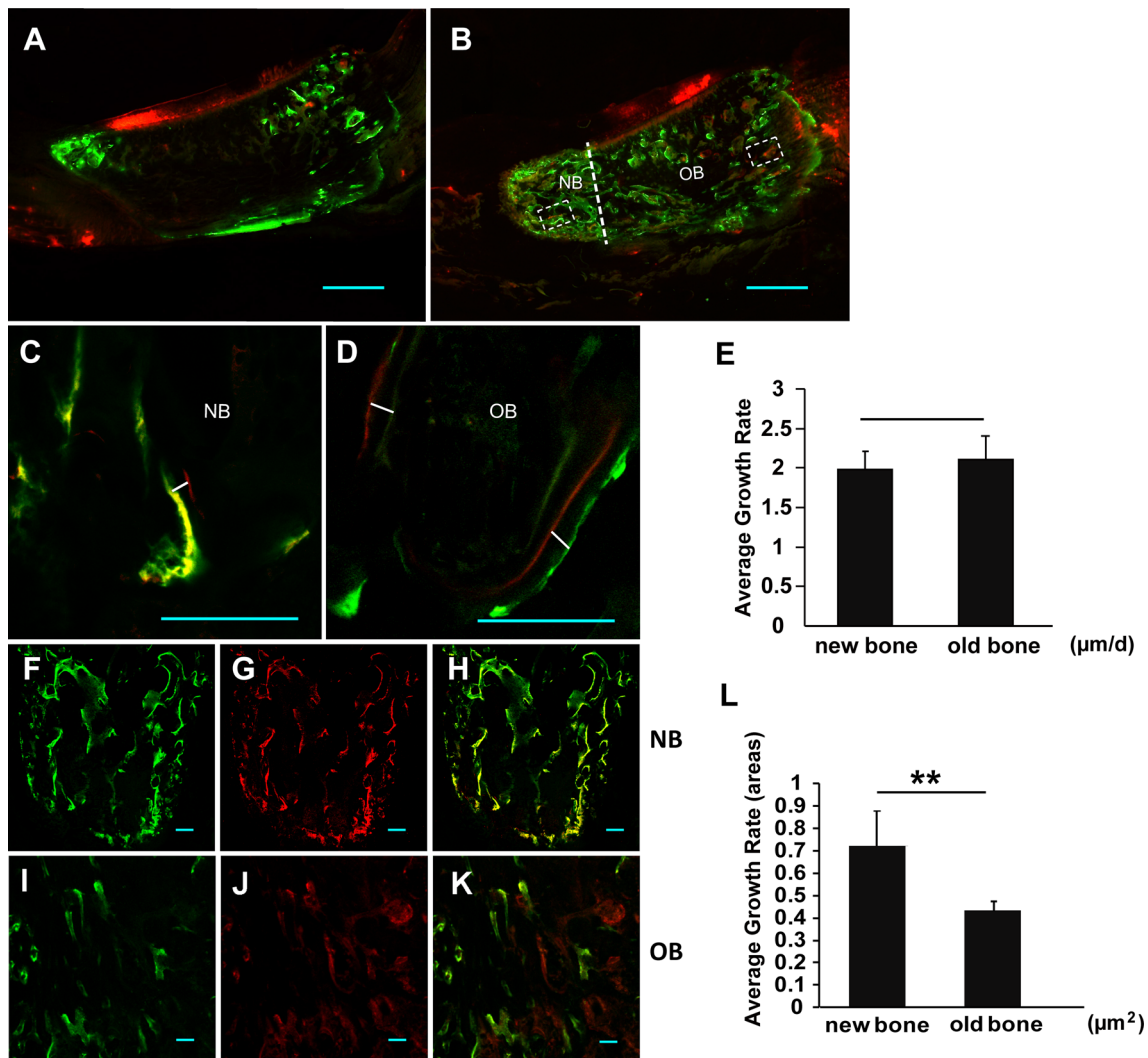


**Fig. 2** Analysis of bone tissue sections using CFM and CLSM. The rabbit patella after partial patellectomy was sagittally sectioned with a thickness of 300 µm. **a, b** CFM image with low magnification of 12.5×. **c–l** CLSM images. **a** CFM image of a normal rabbit patella at a glance. **b** CFM image of the patella 12 weeks after partial patellectomy. **OB** old bone, **NB** new bone. *Dashed line* shows original surgical cutting line of patellectomy; the region containing typical fluorescent labeling lines selected for calculating bone apposition rate is boxed in dashed lines. **c** Magnified NB box in **b** by CLSM showing the two clearly fluorescently labeled lines; the distance between the lines (*white bar*) was measured and used for calculation of bone apposition rate 12 weeks after patellectomy. **d** Magnified OB box in **b** by CLSM displaying the two fluorescently labeled lines in old bone retained from the patellectomy, from which

the distance (*white bar*) was measured for estimation of bone formation rate. **e** Quantitative analysis of bone apposition rates for NB in **c** and OB in **d**, calculated from the measured distances between labeled lines (*white bars*), which shows no significant difference statistically ( $p > 0.05$ ). **f–h** CLSM images of NB 12 weeks after patellectomy. **i–k** CLSM images of OB at 12 weeks postpatellectomy. **f, i** CLSM images acquired using green fluorescence channel (*calcein green*). **g, j** CLSM images acquired using red fluorescence channel (*xylanol orange*). **h, k** Merged images. **l** Differential analysis of the red/green ratio of labeled areas (square micrometers) from control and patellectomy sample sections of five animals, demonstrating a highly significant difference between new bone and old bone (\*\* $p < 0.01$ ). Scale bar = 200 µm

the same time through multiple channels, the fluorescent signals are further processed using specific software to filter out the effects of crosstalk. When the optical “sections” of nondecalcified thick bone with sequential polychromes were observed using CLSM, the laser scanning microscope generated sharp images, which were able to solve the problem of PVEs encountered when using CFM (Fig. 1). The images by MTS were verified by

META, which is a special mode in Zeiss LSM 510 that recognizes signals by the specific pattern of individual wavelength for acquiring pixels, to eliminate crosstalk between fluorescent signals. Although section thickness of <10 µm was previously reported for sharp images by CFM [33], sectioning of bone tissues is difficult without decalcification. Bone quantification studies by CFM require sections of ≥10 µm using a specific heavy-duty microtome

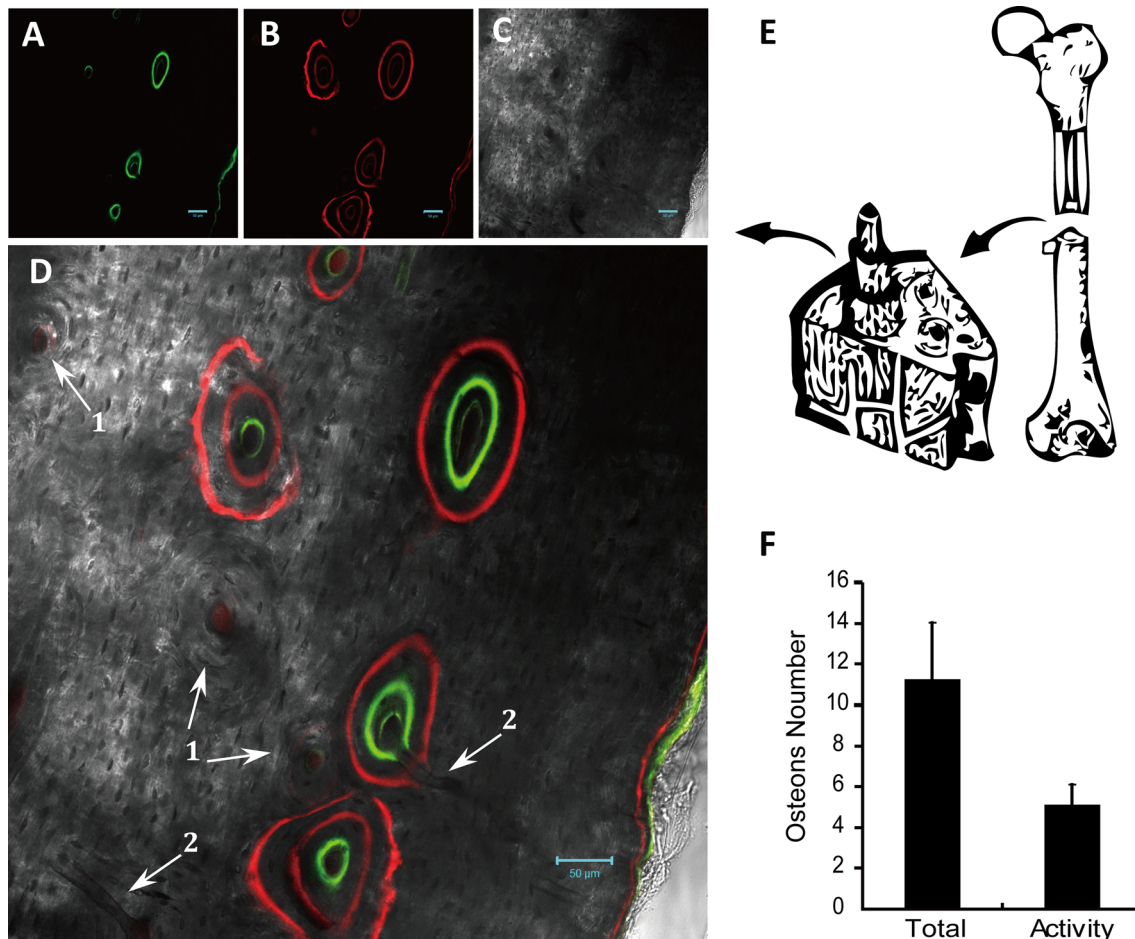


**Fig. 3** Fluorescent images acquired by CLSM plus DIC scanning. Crosscutting section of goat tibia with a thickness of 400  $\mu\text{m}$  in thick bone with a scale of 50  $\mu\text{m}$ . **a** Image acquired by green fluorescence channel. **b** Image acquired by red fluorescence channel. **c** Image acquired by DIC channel. **d** Merged image of three-channel CLSM images (green and red fluorescence +DIC) of **a**, **b**, and **c**. Merged image shows two calcified fluorescent labels from different times (green and red) plus DIC (gray). The weak red color from the second calcein labeling still existed and merged into the first green labeling,

combined into a yellowish color with various intensities depending upon the ratio of the two colors at developmental stages of those osteons. *Arrow 1* indicates quiescent osteons in comparison to the fluorescently labeled active osteons; *arrow 2* points out the Volkmann's channels. **e** A diagrammatic illustration of the anatomical processing of bone specimens. **f** Mean of total osteon numbers versus mean of the active osteon numbers shown on 10 images (views) from five animals at 20 $\times$  magnification labeled with fluorescent dyes and acquired by CLSM combined with DIC

for clear images, and the thin sections are easily broken; and it is difficult to prepare enough sequential sections at this thickness range for nondecalfied bone tissue sections.

CLSM overcomes these difficulties by using thick sections. For bone samples with polychrome sequential labeling, the section thickness scanned by CLSM can be readily adjusted and is more advantageous than CFM, including, as it does, a wider selection of wavelength ranges, high sensitivity, high discriminability, strong contrast, and sharp imaging. Upper and lateral specific ROIs were observed simultaneously, and the depth of the labeled mineralization in a sample layer was shown (Fig. 1d, e). These 3D structures were not readily visualized using CFM. Collectively, CLSM displays superior imaging quality of fluorescent-labeled bone sections and provides

an option for 3D imaging reconstruction. To date, CLSM obtains fluorescently labeled images with a range of wavelengths simultaneously at high sensitivity to distinguish labels with narrow wavelength differences [34, 35].

Normal osteoblasts secrete osteoid that will be mineralized layer by layer with collagen fiber forming pore-like structures aligning parallel to the mineral lamella of 7–10  $\mu\text{m}$  for calcium hydroxyapatite precipitation and crystallization in about 10 days under physiological conditions [11]. Due to the mineralization lag phenomenon, there is a band of osteoid that is formed between the mineralized bone surface and osteoblasts. In vivo, tetracycline and other fluorescent dyes will be deposited in the mineralization front of the ossification surface, the new bone formation being then labeled in experimental animals

treated orally and intravenously with fluorescent labeling agents several times [11]. Calcein green and xylenol orange can specifically bind to calcium deposited on the mineralization front and show bright green and red fluorescent colors under a fluorescence microscope, respectively.

The fluorescently labeled area is related to the amount of combined calcium. Measurement of morphologic components includes direct measurement of static variables and kinetic variables usually generated by fluorescent labels applied at timed intervals and integrated into the forming bones. The distance between different labels reflects the rate of bone formation, and those *in vivo* traces generated by bone remodeling permit dynamic detection and estimation of rates of remodeling activity and active osteons [1]. Mineralization fronts within lamellae of the active osteons in cortical bone were visualized in thin sections by CFM, and their apposition rate was presented as the distance between the fluorescent bands over the number of days after *in vivo* injection of polychrome fluorescence dyes and further used for the estimation of new bone formation rate in intact bones [1, 31]. CLSM observations (Fig. 2c–e) in this study suggest that the conventional bone mineral apposition rate calculated by measuring the distance between two parallel labeling bands can be more precisely defined without PVE when compared with CFM in intact bone. However, the bone mineral apposition rate by distance measurement in healing bones was even slower than that for intact or old bone, suggesting a limitation in its application in studying healing bone mineral apposition. This finding was also consistent with other observations by CFM where the new bone formation rate was found to be far higher than that of the remodeling shown in old bones in our previous study [27]. There were no significant differences in bone apposition rate detected during the bone repairing of sesamoid bone as compared to normal bone formation by the CFM-based measurement (Fig. 2e). In fact, the new bone formed around the residual proximal patella after partial patellectomy showed no regular bone plate structure and typical mineralization fronts by CLSM (Fig. 2f–h). The new bone growth after surgery and fracture repair is rapid in overlapped reticular formats, showing blurred images under CFM (no effect of signal crosstalk), which is different from the normal bone development and cannot form clearly separated decalcification bands. The conventional distance measurement approach is not applicable for evaluation of new bone formation and its remodeling in healing bones, e.g., in fracture repair where it undergoes rapid osteogenesis or new bone formation with irregular mineral deposition and integration of disorganized collagen fibers as shown in the partial patellectomy rabbit model of this study.

Images of fluorescent labels in the field of newly formed bone were acquired by CFM individually using filters in

thin sections. Fluorescent signals were quantified and interpreted as ratio of labeled areas with xylenol orange and calcein green to study the dynamics of osteogenesis and its remodeling [6]. The quantification and calculation of labeled areas in images obtained using CLSM easily were more accurate on an optical section of thick tissues. Eventually, significant differences in labeled areas of calcein green and xylenol orange were detected (Fig. 2l) between the new bone and the old bone. Altogether, the ratio of labeled areas calculated by CLSM recorded differential outcomes on progressive new bone formation during repair of sesamoid bone as compared to normal bone formation, which is not readily appreciated by CFM-based technique. CLSM allows one to define the fluorescent labels in the lamellar diffusion type and linear margin during new bone formation. The results of this work suggest that fluorescence intensity measurements as mean areas using CLSM is a better option to conventional distance measurement and the area ratio calculation for analyses of new bone formation in repair.

DIC technology was originally used to observe the structure of histological sections without staining by the supplementation of a pair of polar elements and a Wollaston glass prism in the phase-contrast microscope to increase the contrast of interface characteristics of specimens [11, 36]. The related data of the fluorescence image and the DIC image can be obtained in the same procedure, and the overlapped images are accurately distinguished by their repeatable confocal measurements [37]. Densities of bone samples can be precisely detected using X-ray and CT scanning, but those methods are not suitable for demonstrating the activeness of bone cells at a given developing stage. Investigations on thick nondecalcified bone samples were rarely reported previously. Calcification *in vivo* is a dynamic process; the number and density of labeled bands represent the levels of calcification at a particular time, which makes labels and density different even in the same sample with no labels for quiescent osteons at a particular developmental stage (Fig. 3). This study used the CLSM technique combined with DIC to localize the mineralized bone matrix labeled with multiple fluorescent dyes. In particular, introduction of the DIC technique to the study of the dynamics of osteons enables the precise localization of the mineralized front with polychrome sequential labeling in thick nondecalcified bone sections; this not only localized the calcified labels but also revealed the relations between morphology and function according to the activeness of osteons. The beginning and the stages of new bone formation can be determined by color integrations. Application of the fluorescent labeling technique combined with DIC in this report ascertains a combined microscopic interpretation for research of bone development, which is instructively significant for thick bone samples compared



to samples of conventional cell cultures. Further development of CLSM and the DIC technique might provide a new image-processing protocol for the study of bone mineral metabolism and healing in calcified tissue research.

In summary, new bone formation and bone microstructure, including the mineralization fronts, were investigated by CLSM, which showed an advantage in adjustments of operating parameters, thickness of optical sections, and automatic image acquisition and analysis. Polychrome sequential fluorescence quantification is more accurate with higher repetitiveness than CFM and area ratios of sequential fluorescent labels in new bone formation by CLSM in healing bone was calculated as new bone growth rate, a better estimation of bone growth in repair. CLSM combined with DIC further generated sequentially fluorescent images showing mineral apposition with details of microstructure, including osteons and Volkmann's channel. The presence or absence of fluorescent labels in osteons reflects their activeness during bone formation and remodeling, which renders a new imaging process for the study of bone mineral metabolism and fracture healing.

**Acknowledgments** This study was made possible by the financial support of a Hong Kong RGC Earmarked Research Grant (4155/02 M), Guangdong Natural Science Foundation Grant (S2012010010616), Key Project of Guangzhou Medical Health Science and Technology (20121A021009), and Science and Technology Project funded by the Guangzhou municipal government (2012J4100027). We are grateful to Dr. K. F. Tam for kindly making the bone samples available and Dr. J. W. Chen for advice on hard tissue sample preparation, both from the Department of Orthopaedics and Traumatology of the Chinese University of Hong Kong.

## References

- Eriksen EF, Axelrod DW, Melsen F (1994) Bone histomorphometry. Raven Press, New York
- Mohsin S, O'Brien FJ, Lee TC (2006) Microcracks in compact bone: a three-dimensional view. *J Anat* 209:119–124
- Lee TC, Arthur TL, Gibson LJ, Hayes WC (2000) Sequential labelling of microdamage in bone using chelating agents. *J Orthop Res* 18:322–325
- Serra G, Morais LS, Elias CN, Meyers MA, Andrade L, Muller CA, Muller M (2010) Sequential bone healing of immediately loaded mini-implants: histomorphometric and fluorescence analysis. *Am J Orthod Dentofacial Orthop* 137:80–90
- Pautke C, Vogt S, Tischer T, Wexel G, Deppe H, Milz S, Schieker M, Kolk A (2005) Polychrome labeling of bone with seven different fluorochromes: enhancing fluorochrome discrimination by spectral image analysis. *Bone* 37:441–445
- Lu H, Qin L, Fok P, Cheung W, Lee K, Guo X, Wong W, Leung K (2006) Low-intensity pulsed ultrasound accelerates bone–tendon junction healing: a partial patellectomy model in rabbits. *Am J Sports Med* 34:1287–1296
- Pautke C, Vogt S, Kreutzer K, Haczek C, Wexel G, Kolk A, Imhoff AB, Zitzelsberger H, Milz S, Tischer T (2010) Characterization of eight different tetracyclines: advances in fluorescence bone labeling. *J Anat* 217:76–82
- Hoffman EJ, Huang SC, Phelps ME (1979) Quantitation in positron emission computed tomography: 1. Effect of object size. *J Comput Assist Tomogr* 3:299–308
- Pretorius PH, King MA (2009) Diminishing the impact of the partial volume effect in cardiac SPECT perfusion imaging. *Med Phys* 36:105–115
- Pawley JB (2006) Handbook of biological confocal microscopy. Springer, New York
- Li N, Yi L, Su Z (1997) Laser scanning confocal microscopic technology. People's Military Medical Press, Beijing in Chinese
- Okuda K, Nakajima Y, Irie K, Sugimoto M, Kabasawa Y, Yoshie H, Hara K, Ozawa H (1995) Transforming growth factor-beta 1 coated beta-tricalcium phosphate pellets stimulate healing of experimental bone defects of rat calvariae. *Oral Dis* 1:92–97
- Grotz KA, Piepkorn B, Al-Nawas B, Duschner H, Bittinger F, Kann P, Beyer J, Wagner W (1999) Confocal laser scanning microscopy: a nondestructive subsurface histotomography of healthy human bone. *Calcif Tissue Int* 65:8–10
- Doube M, Firth EC, Boyde A (2005) Registration of confocal scanning laser microscopy and quantitative backscattered electron images for the temporospatial quantification of mineralization density in 18-month old thoroughbred racehorse articular calcified cartilage. *Scanning* 27:219–226
- Roelofs AJ, Stewart CA, Sun S, Blazewska KM, Kashemirov BA, McKenna CE, Russell RG, Rogers MJ, Lundy MW, Ebetino FH, Coxon FP (2012) Influence of bone affinity on the skeletal distribution of fluorescently labeled bisphosphonates in vivo. *J Bone Miner Res* 27:835–847
- Iyama S, Takeshita F, Ayukawa Y, Kido MA, Suetsugu T, Tanaka T (1997) A study of the regional distribution of bone formed around hydroxyapatite implants in the tibiae of streptozotocin-induced diabetic rats using multiple fluorescent labeling and confocal laser scanning microscopy. *J Periodontol* 68:1169–1175
- Nishikawa T, Masuno K, Mori M, Tajime Y, Kakudo K, Tanaka A (2006) Calcification at the interface between titanium implants and bone: observation with confocal laser scanning microscopy. *J Oral Implant* 32:211–217
- Boyde A, Lovicar L, Zamecnik J (2005) Combining confocal and BSE SEM imaging for bone block surfaces. *Eur Cells Mater* 9:33–38
- Vukojević V, Heidkamp M, Ming Y, Johansson B, Terenius L, Rigler R (2008) Quantitative single-molecule imaging by confocal laser scanning microscopy. *Proc Natl Acad Sci USA* 105:18176–18181
- Czymmek KJ, Whallon JH, Klomparens KL (1994) Confocal microscopy in mycological research. *Exp Mycol* 18:275–293
- Spear RN, Cullen D, Andrews JH (1999) Fluorescent labels, confocal microscopy, and quantitative image analysis in study of fungal biology. *Methods Enzymol* 307:607–623
- Williams DA (1990) Quantitative intracellular calcium imaging with laser-scanning confocal microscopy. *Cell Calcium* 11:589–597
- Raarup MK, Nyengaard JR (2011) Quantitative confocal laser scanning microscopy. *Image Anal Stereol* 25:111–120
- Verschure PJ, van Marle J, Joosten LA, Van den Berg WB (1994) Localization and quantification of the insulin-like growth factor-1 receptor in mouse articular cartilage by confocal laser scanning microscopy. *J Histochem Cytochem* 42:765–773
- Verschure PJ, Van Marle J, Van Noorden CJ, Van den Berg WB (1997) The contribution of quantitative confocal laser scanning microscopy in cartilage research: chondrocyte insulin-like growth factor-1 receptors in health and pathology. *Microsc Res Tech* 37:285–298
- Tam KF, Cheung WH, Lee KM, Qin L, Leung KS (2009) Shockwave exerts osteogenic effect on osteoporotic bone in an ovariectomized goat model. *Ultrasound Med Biol* 35:1109–1118

27. Qin L, Fok P, Lu H, Shi S, Leng Y, Leung K (2006) Low intensity pulsed ultrasound increases the matrix hardness of the healing tissues at bone–tendon insertion—a partial patellectomy model in rabbits. *Clin Biomech (Bristol, Avon)* 21:387–394
28. Lui P, Zhang P, Chan K, Qin L (2010) Biology and augmentation of tendon–bone insertion repair. *J Orthop Surg Res* 5:59
29. Lu H, Qin L, Lee K, Cheung W, Chan K, Leung K (2009) Identification of genes responsive to low-intensity pulsed ultrasound stimulations. *Biochem Biophys Res Commun* 378:569–573
30. Qin L, Mak AT, Cheng CW, Hung LK, Chan KM (1999) Histomorphological study on pattern of fluid movement in cortical bone in goats. *Anat Rec* 255:380–387
31. Clark PA, Rodriguez A, Sumner DR, Hussain MA, Mao JJ (2005) Modulation of bone ingrowth of rabbit femur titanium implants by in vivo axial micromechanical loading. *J Appl Physiol* 98:1922–1929
32. Zarrinkalam KH, Kuliwaba JS, Martin RB, Wallwork MA, Fazzalari NL (2005) New insights into the propagation of fatigue damage in cortical bone using confocal microscopy and chelating fluorochromes. *Eur J Morphol* 42:81–90
33. Kazama JJ, Gejyo F, Ejiri S, Okada M, Ei I, Arakawa M, Ozawa H (1993) Application of confocal laser scanning microscopy to the observation of bone biopsy specimens. *Bone* 14:885–889
34. Muller M (2006) Introduction to confocal fluorescence microscopy, 2nd edn. International Society for Optical Engineering, Washington DC
35. Matsumoto B (2002) Cell biological applications of confocal microscopy, 2nd edn. Academic Press, Elsevier Sciences, New York
36. Guo S, Luo X, Qiu G (2001) Clinical basis of osteoporosis. Tianjin Science and Technology Press, Tianjin in Chinese
37. Sahara M, Sata M, Matsuzaki Y, Tanaka K, Morita T, Hirata Y, Okano H, Nagai R (2005) Comparison of various bone marrow fractions in the ability to participate in vascular remodeling after mechanical injury. *Stem Cells* 23:874–878